 FDMP, vol.13, no.4, pp.221-234, 2017

Numerical Analysis on Unsteady Internal Flow in an Evaporating Droplet

Zhentao Wang[1], *, Kai Dong and Shuiqing Zhan

Abstract: We have investigated the unsteady internal flow occurring in an evaporating droplet interacting with a high-temperature atmospheric environment. The Navier-Stokes equations for both the liquid and the gas phases have been solved numerically in the framework of a Volume of Fluid (VOF) method relying on the so-called Continuum Surface Force (CSF) model. A specific kernel able to account for evaporation and related phase change has been incorporated directly in the VOF approach. The temperature distributions within the droplet has been found to be relatively uniform by virtue of the Marangoni flow. The transient evolution of the flow pattern and related heat exchange effects have been also investigated.

Keywords: Internal circulation, droplet evaporation, Volume of Fluid (VOF) method, Continuum Surface Force (CSF) model, Marangoni flow.

Nomenclature

A=	Interface area, m^2
c_p=	Heat capacity, $J\ kg^{-1}\ K^{-1}$
C_p=	Surface pressure coefficient
d=	Diameter of vapor bubble, m
f_σ=	Volumetric force, N
g=	Gravity, $m\ s^{-2}$
k=	Thermal conductivity, $W\ m^{-1}\ K^{-1}$
L=	Latent heat of vaporization, $J\ kg^{-1}$
m=	Mass, kg
M=	Relative Molecular weight
p=	Pressure, p_a
q=	Heat flux, $W\ m^{-2}$
S=	Stress tensor, $N\ m^{-2}$
r*=	Relative coordinate
R=	Universal gas constant, $J\ K^{-1}\ mol^{-1}$
R_e=	Reynolds number
t=	Time, s
T=	Temperature, K

[1] School of Energy and Power Engineering, Jiangsu University, 301 Xuefu Road, Zhenjiang, Jiangsu 212013, China.

* Corresponding author: Zhentao Wang. Email: zhentao.wang@ujs.edu.cn.

u= Velocity, $m\ s^{-1}$
V_{cell}= Cell volume, m^3
x, y = Coordinate

Greek symbols
α= Liquid volume fraction
β= Accommodation coefficient
μ= Dynamic viscosity, $kg\ m^{-1}\ s^{-1}$
κ= The curvature of the interface region
v= Specific volume, $m^3\ kg^{-1}$
ρ= Density, $kg\ m^{-3}$
σ= Surface tension coefficient, $N\ m^{-1}$

1 Introduction

Liquid is ubiquitously evaporated in nature and human activities, and such course has been extensively adopted in industry, including refrigeration, printing, coating, and production of novel materials [Park and Lee (2003); Buffone and Sefiane (2004)]. The evaporation of droplets across the interface is of critical significance for numerous scientific and industrial applications [Niazmand, Shaw, Dwyer et al. (1994); Gleason, Voota and Putnam (2016); Rybdylova, Poulton, Qubeissi et al. (2018)]. The typical examples in nature refer to the growth of rain drops stemmed from condensation, and the evaporation of fuel droplets in the course of combustion, and also have been massively analyzed in engineering. Droplets evaporation is also underlying to manage and control thermal energy in the microgravity environment. The droplet evaporation and internal circulation were reckoned with by several investigators [Zhang and Yang (1992); Shih and Megaridis (1996); Hu and Larson (2005); Lu, Duan, Wang et al. (2011)], whereas thermocapillary (Marangoni) effects were generally neglected in most of the previous work [Bénard (1901); Pearson (1958); Hu and Larson (2005)].

Marangoni effects were observed in the early 1800s and known as “tears of wine” [Hu and Larson (2005)]. These surface effects induced by a surface tension gradient were elucidated by Italian physicist Marangoni, which could be generated either by temperature or by composition difference. Such phenomenon was also detected in a thin film [Bénard (1901)]. Besides, various Marangoni flows in thin film and shallow pools have been experimentally and theoretically studied in numerous works [Block (1956); Pearson (1958); Soltani and Rahal (2017)]. Marangoni flow in an evaporating droplet has been reported in several literatures. The liquid fuel droplet heating and internal circulation was firstly probed into by Prakash et al. [Prakash and Sirignano (1978)]. Marangoni flow was observed in natural convection of evaporating drops by Zhang et al. [Zhang and Yang (1992)], and they also uncovered the existence of three structured of distinct flow at the liquid air interface, i.e. the stable, substable and unstable structures. A computational model of transient droplet vaporization was presented by Niazmand et al. [Niazmand, Shaw, Dwyer et al. (1994)], and the surface tension gradients impacted the velocity fields and

temperature of droplets evidently, as accordingly found. The thermocapillary convection effect exerted on the dynamics behavior taken on by vaporizing-convective hydrocarbon droplet was numerically investigated by Shih et al. [Shih and Megaridis (1996)], and the surface tension gradients facilitated droplet internal circulation and shortened the evaporation time, as the model predicted. The natural convective flow in the evaporating droplet was probed into by Hegseth et al. [Hegseth, Rashidnia and Chai (1996)], and the energetic convective flow was also ascertained. The life time and stability taken on by an evaporating droplet were analyzed. The evaporation of hanging drops was studied by Savino et al. [Savino, Paterna and Favaloro (2002)], and the impact exerted by Marangoni convection and buoyancy on the droplet evaporating was also discussed [Savino and Fico (2004)]. The impacts exerted by Marangoni stresses on the flow in an evaporating sessile droplet were studied by Hu et al. [Hu and Larson (2005)]. The evaporating dynamics and convection flow in water drops were analyzed by Girard et al. [Girard, Antoni, Faure et al. (2006)], and the Marangoni effects on the evaporation rates were also discussed [Girard, Antoni and Sefiane (2008)]. The evaporating of drops of air flow in atmospheric environment was numerically investigated by Schlottke et al. [Schlottke and Weigand (2008)], and two pair vortexes were formed inside drop, as accordingly found. The contact angle behavior taken on by pendant and sessile evaporating drops in microgravity environment was experimentally ascertained by Zhu et al. [Zhu, Brutin, Liu et al. (2010)]. The evaporation of a liquid on a heated solid surface was numerically analyzed by Lu et al. [Lu, Duan, Wang et al. (2011)] through adopting a comprehensive model, and the internal flow was discussed with the impacts exerted by buoyancy force, thermocapillary force and viscous resistance factored in. The internal circulation in an evaporating drop was anatomized by Mandal et al. [Mandal and Bakshi (2012)], and the evaporation could induce the internal flow, as accordingly found. In the meantime, evaporating rate could be increased further than that in the diffusion-driven evaporation under the atmospheric environment. The evaporation and convective flow pattern taken on by a heated pendant silicone oil droplet have been anatomized in the case of the steady-state conditions [He and Duan (2015)]. Most literatures discussed the steady internal flow in evaporating droplets with Marangoni effects factored in, though some apparent progresses have been made in evaporating droplets taking on internal circulation.

An evaporating droplet was usually hanging on the heated supporter or being placed on the heated substrates in ambient temperature in previous studies. In these cases, steady Marangoni flow should be attained arising from the steady temperature gradients on the droplets surface. Yet steady temperature gradients fail to be induced on droplet surface arising from the extremely short lifetime of droplet, and the steady Marangoni convection fails to be formed either as a droplet is suspending under the high-temperature atmospheric environment. In this paper, Volume of Fluid (VOF) method is employed to track gas and liquid interface, and Continuum Surface Force (CSF) model is adopted to present the surface tension on the interface. Furthermore, the unsteady circulation flow and surface temperature distributions were presented, and the Marangoni effects in unsteady process were discussed.

2 Numerical models

2.1 VOF model

The unsteady internal flow in an evaporating droplet suspended under high-temperature atmospheric environment, is commonly deemed 2D. The liquid volume fraction, denoted by α, is introduced adopting the Volume of Fluid (VOF) method to distinguish between the gas and the liquid phases [Hirt and Nichols (1981); Schlottke and Weigand (2008)]. The liquid volume fraction α is defined as:

$$\alpha = \frac{\text{volume of liquid phase}}{\text{total volume of control volume}} \tag{1}$$

where the α-function equals to:

$$\alpha(x,t) = \begin{cases} 1, \text{for a point } (x,t) \text{ in liquid phase} \\ 0, \text{for a point } (x,t) \text{ in gas phase} \\ 0 < \alpha < 1, \text{for a point } (x,t) \text{ in the interface between gas and liquid} \end{cases} \tag{2}$$

where, α denotes the liquid volume fraction. An explaining illustration is presented in Figure 1. The phase change is involved in transport equation of the liquid volume fraction α, which is expressed as

$$\frac{\partial \alpha}{\partial t} + \nabla(\alpha \vec{u}) = \frac{1}{\rho_l} \frac{\dot{m}_{evap}}{V_{cell}} \tag{3}$$

The momentum equation is defined as

$$\frac{\partial(\rho \vec{u})}{\partial t} + \nabla \cdot (\rho \vec{u} \vec{u}) = -\nabla p + \nabla \cdot \mu \vec{S} + \vec{f}_\sigma \tag{4}$$

where, $\vec{S}$ denotes stress tensor, $\vec{u}$ refers to velocity and f_σ represents volumetric force given the surface tension following Continuum Surface Force (CSF) model [Brackbill, Kothe and Zemach (1992)]. The f_σ value equals to $f_\sigma = \sigma \cdot \kappa \cdot (\nabla \alpha)$, where, σ denotes surface tension coefficient and κ refers to the curvature of the interface region.

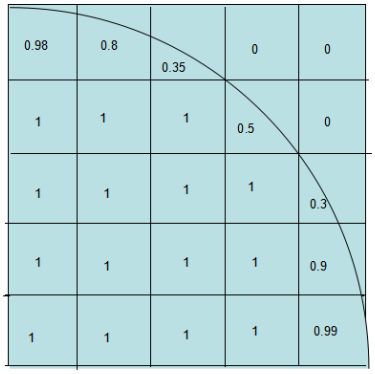

Figure 1: Volume fraction in each cell

The energy transport equation is expressed as

$$\rho c_p \frac{DT}{Dt} = \nabla(k\nabla T) + \frac{Dp}{Dt} - \frac{\dot{m}_{evap} L}{V_{cell}} \tag{5}$$

where, c_p refers to heat capacity, T bespeaks temperature, k denotes thermal conductivity, L indicates the latent heat of vaporization, V_{cell} bespeaks the cell volume, p refers to pressure.

2.2 Evaporation model

The model employed abides by the formula presented by Hertz Knudsen,

$$q_{\dot{m}} = \beta \sqrt{\frac{M}{2\pi R T_{sat}}} (p - p_{sat}) \tag{6}$$

Where, β denotes the so-called accommodation coefficient, M refers to relative Molecular weight, R indicates universal gas constant, T_{sat} refers to saturated temperature, p represents the vapor partial pressure, and p_{sat} bespeaks saturated pressure. The interface is assumed saturated. The Clapeyron-Clausius equation expressing how the pressure and the temperature are related under the saturation condition is expressed as

$$\frac{dp}{dT} = \frac{L}{T(v_g - v_l)} \tag{7}$$

where, v denotes the specific volume, and v_l is negligible compared with v_g. Incorporating Eq. (7),

$$p - p_{sat} = \frac{L}{v_g} (\ln T - \ln T_{sat}) \tag{8}$$

Combined Eqs. (6) and (8),

$$q_{\dot{m}} = \beta \sqrt{\frac{M}{2\pi R T_{sat}}} L \rho_g (\ln T - \ln T_{sat}) \tag{9}$$

The diameter of vapor bubble is proved identical, and the interface area is expressed as

$$\frac{A_i}{V_{cell}} = \frac{6\alpha_g}{d} \tag{10}$$

where, V_{cell} denotes the volume of cell and the phase source (kg/s $\cdot$m^3) can be expressed as

$$\dot{m}_{evap} = q_{\dot{m}} \frac{A_i}{V_{cell}} == \frac{6}{d} \beta \sqrt{\frac{M}{2\pi R T_{sat}}} L \left[\rho_g \alpha_g (\ln T - \ln T_{sat})\right] \tag{11}$$

It is given as,

$$\varsigma_{coe} = \frac{6}{d} \beta \sqrt{\frac{M}{2\pi R T_{sat}}} L \tag{12}$$

The mass source phase is expressed in the form,

$$\dot{m}_{evap} = \varsigma_{coe} \cdot \alpha_g \rho_g (\ln T - \ln T_{sat}) \tag{13}$$

2.3 Physical model

Figure 2 illustrates a schematic two-dimensional (2D) computational model. The numerically simulated region is selected as $10\times10R$ in this paper. The computational domain is sufficient to ensure the evaporation and internal velocity within droplet to be not impacted by boundary conditions. An evaporating droplet suspended under an atmospheric environment and taking on 1.0 mm radius R and 998 kg/m^3 density is assumed. The computational domain contains two different fluids, i.e. the liquid (droplet) and gas (atmospheric air) phases. The initial state of droplet is spherical and assumed at the center of the gas phase. The ambient temperature of atmospheric air is promptly elevated as 500 K. The gravity is ignored. Figure 2 illustrates the physical model. The grids are generated with Gambit and constructed as the orthogonal grid system. Numerical study is conducted in this paper adopting the commercial CFD software FLUENT. The equations are discretized over the computational domain whereby a finite volume method. Convection and diffusion terms are discretized employing the second-order upwind schema. The two-phase flow field is calculated in line with the pressure implicit splitting of operator (PISO) algorithm established on the basis of the transient problems. The iteration time is 10-6e s to ensure the accurate capture of internal circulation and interface change.

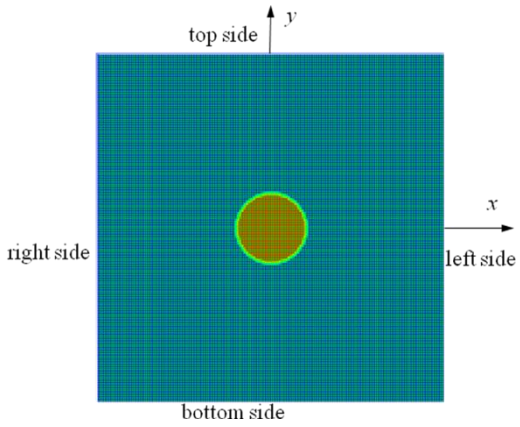

Figure 2: The model and orthogonal grid system

2.4 Grid independence

The size and number of selected grids commonly exert evident impact on the calculated results, inclusive of velocity and temperature distribution. The grid independence was studied. The three-grid systems of grids1 (8300), grids2 (23200) and grids3 (53828) are employed at R_{eg}=40 (Figure 3a and b). Figure 3a presents the comparison of the predicted pressure coefficient (C_p, Eq. (14)) along a cylinder surface for the case of R_{eg}=40. As evidently indicated, the similar results were attained by the three grids. To save the memory and computing time, the number of grids is established as smaller. A comparison of the pressure distribution along a cylinder surface at R_{eg}=40 with prior experimental and theoretical studies, are also performed and a good consistency was obtained [Grove, Shair, Petersen et al. (1964); Chen (2001)]. The present model is indicated accurate to predict

convective behaviors of a droplet.

$$C_p = \frac{2(p_s - p_\infty)}{\rho_g u_\infty^2} \tag{14}$$

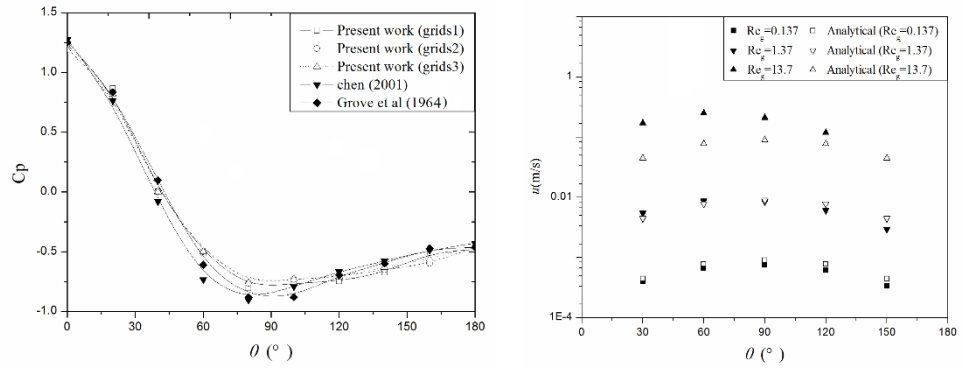

(a) (b)

Figure 3: Comparisons of present and previous work (a) surface pressure coefficients and (b) surface velocity

Figure 3b presents the predicted and analytical surface velocity in the case of different Reynolds numbers [Wang, Guo, Tian et al. (2017)]. An approximated sinusoidal function of the surface velocity is indicated in Figure 3b and the strength taken on by the internal vortex can be characterized by the droplet interfacial velocity. Given that the analytical solution is merely for low Reynolds numbers, the predicted values are approaching to analytical values under lower Reynolds number, whereas discrepant in larger Reynolds number. The diameter perpendicular to the flow direction counts as the symmetrical axis, in which generates a front and rear sections of the droplet. The velocity in the droplet is not symmetrically distributed in the front and rear sections, as indicated from the figure. A larger velocity distributed is observed in the front section, whereas a lower one appears in the rear section. This arises from an unsymmetrical friction experienced by the front and rear sections of the droplet, and more significant to the droplet at higher Reynolds number.

3 Results and discussion

3.1 Droplet on the heated substrate

This paper first numerically studies the internal circulation in an evaporating ethanol droplet with 1.0mm radius *R* on the heated solid surface. The surface tension is assumed to be a function of temperature, which is expresses as

$$\sigma = \sigma_0 - \sigma_T (T - T_0) \tag{15}$$

where, σ_0 of 0.0223 N/m denotes value of surface tension at temperature of 298.0 K, σ_T of 8.07-e5 N/(m Ⱪ) bespeaks the coefficient. A schematic 2D axisymmetric computational model would be resolved in this chapter. The *x*-axis is established as a heated solid substrate, the top side as wall, the right side as pressure inlet, while the left side as pressure outlet.

The ethanol droplet shall be heated by hot solid substrate. The temperature of heated solid plate is established at 333.0 K.

Figure 4 presents the streamlines of internal circulation and temperature contours of numerical results. Figure 5a plots the temperature distribution on right part of droplet surface, the r^* denotes the relative coordinate and is defined as

$$r^* = \frac{x}{R} \tag{16}$$

where, x denotes value of horizontal coordinate, R refers to droplet radius connected with substrate. $r^*=0$ denotes the top of the droplet, while $r^*=1$ denotes the edge of the droplet at R. The temperature is diversified on the droplet surface because the droplet and evaporation of droplet are heated by substrate, as evidently indicated. The temperature reaches the lowest on the top of the droplet, while the temperature is higher approaching to the substrate. The temperature gradients shall be generated along the droplet surface, Marangoni stresses shall be induced, and the surface motion shall be generated from high to low temperature areas. The droplets surface driving the surrounding fluid, the internal circulation vortex shall be formed, and as exhibited in Figure 4a. The evaporation rate shall increase arising from internal circulation vortex, as the heat would be transferred from the bottom to the top of the droplet. Figure 4b presents the temperature contours in the droplet. The temperature is apparently affected by velocity field, as evidently bespoken. There are two temperature vortexes located the same position with identical shape and jointly consistent with the previous work [Hu and Larson (2005); Xu and Luo (2007); Gao, Yin and Hu (2008)]. To assess the impact exerted by Marangoni flow on the evaporating rate, a different model factoring out Marangoni effects has also been adopted to calculate the identical problem. Figure 5a presents how the temperature is distributed on the droplets surface. The temperature increases along the surface of droplet (from the bottom to the top), as evidently indicated. Figure 5b presents the volume variation of the droplet for two different models. As evidently indicated from the results, the evaporation rate with Marangoni effect surmounts that without Marangoni effects. The Marangoni effects are conducive to the evaporation rate much more with the increase of time, and shall not be neglected in droplet evaporating. For instance, when time of 30.0 s, the volume of droplet is 19.2% of original volume with Marangoni effects being taken into account, while 61.8% of original volume with no Marangoni effects.

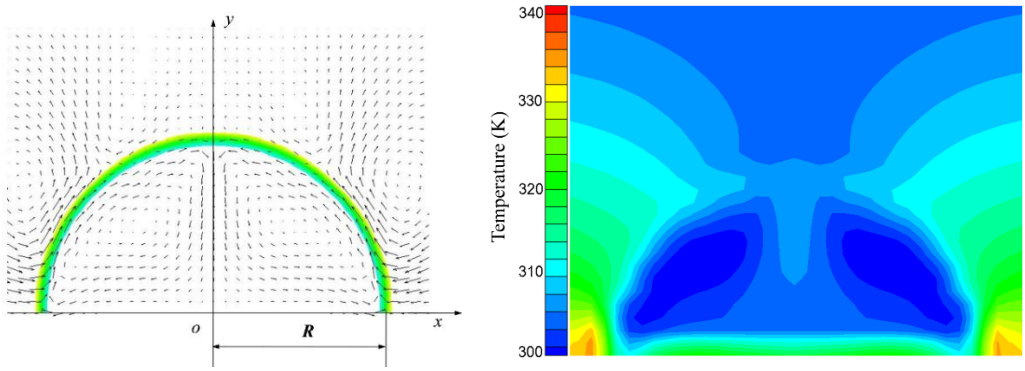

(a) (b)

Figure 4: Internal circulation and temperature contours (a) internal circulation and (b) temperature

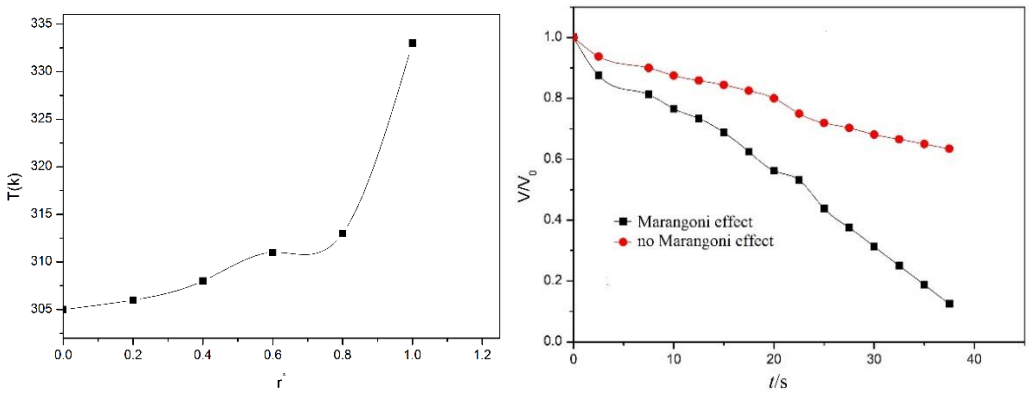

(a) (b)

Figure 5: Drop volume and surface temperature (a) surface temperature distribution and (b) volume changes for two models

3.2 Droplet suspending in the air

The driven forces of the internal circulation in an evaporating droplet are comprised of Marangoni stresses originated from temperature gradients and viscous forces arising from relative motion between two phases. In this paper, merely Marangoni stresses are involved on the interface. Accordingly, both the top and the bottom sides are established as wall. The left side and right side are established as pressure inlet and outlet, respectively. The initial state of droplet is spherical and assumed at the center of the gas phase. The ambient temperature of atmospheric air promptly increases to 500K. And the buoyancy effect is neglected as the gravity is factored out. The surface tension is a function of temperature and is expressed in the form,

$$\sigma = 0.09749404 - 1.396\times10^{-5}T - 2.4\times10^{-7}T^2 \quad (17)$$

T is interface temperature. The local temperature distributions are different arising from different local interface evaporation rates. As a result, the surface tension varies with the

droplet surface. The Marangoni effect would be involved arising from different surface tension. The interface flow from high- to low- temperature areas would be formed, which is named as Marangoni (convective) flow. On the other hand, the convective flow makes the temperature uniform within the droplet, which consequently reduces the surface tension gradients with respect to the original value. The existence of Marangoni flow could improve heat and mass transfer, while uniform temperature tendency makes convective flow instable. When the temperature is constant, the Marangoni flow would vanish, and finally the internal circulation is formed.

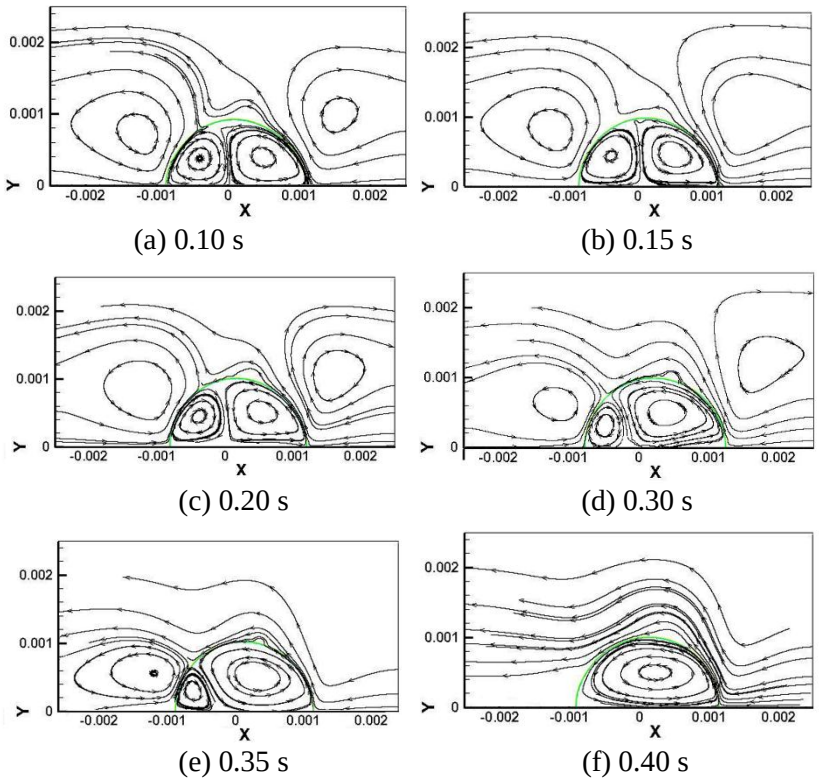

(a) 0.10 s (b) 0.15 s

(c) 0.20 s (d) 0.30 s

(e) 0.35 s (f) 0.40 s

Figure 6: Flow patterns and streamlines (a) 0.10 s, (b) 0.15 s, (c) 0.20 s, (d) 0.30 s, (e) 0.35 s and (f) 0.40 s

3.3 Internal unsteady flows

The lifetime of a droplet with 1.0 mm radius is approximately 3.30 s as a droplet suspending in the still atmospheric air has no relative movements to air, in line with the classical evaporation model. Different flow patterns are found in an evaporating drop as time increases, as presented in Figure 6. The transient streamlines in different moments are illustrated, and unsteady internal flow in an evaporation droplet could be can in this evaporation of droplet. The convective flows would be formed in comparatively short period. The four vortexes are formed arising from the Marangoni effects in Figure 6. From t=0.10 s to 0.25 s, the flow patterns were rarely changed, while t=0.30 s, the right two vortexes turned out to be smaller and the left vortexes turned in excess of original state. For t=0.35 s, the right two vortexes turned even smaller, and the left vortexes turned even larger. The two internal circulations would be formed at t=0.40 s. From t=0.10 s to 0.40 s, the unsteady internal flows is clearly presented in Figure 6, which is from typical convective flows to internal circulations.

Following the foregoing discussion, Marangoni stresses shall be induced by temperature gradients on the droplet surface. In the meantime, the convective flows would be generated. How the convective flow is oriented is commonly dependent on the temperature distribution on the drop surface. Figure 7 illustrates the temperature distributions on the upper half surface of droplet at various moments. For 0.10 s of time, lager gradients of temperature are generated on the right and left ends of drop surface, which shall generate larger gradients of surface tension force, as illustrated in Figure 6. The flow on the drop surface from high to low temperature areas shall be driven by the foregoing force gradients. Furthermore, the convective flow inside droplet shall be driven by the fluid on the surface. The direction of convective flow in the first and third quadrant is counterclockwise, while in the second and fourth quadrant is clockwise, as rectangular coordinate system is established (Figure 2), and the center of droplets counts as the origin of coordinates. Besides, the fluid viscous force originated from inner droplet shall block the movement of fluid on the drop surface. The larger temperature gradients can expedite the motion of fluid at the right and left ends of drop surface. Conversely, the drop surface velocity decreases progressively at the rest areas of drop surface arising from the smaller gradients of surface tension, as illustrated in Figure 7. The velocity on the surface would achieve zero at two different points named as stagnation points on the interface, where the fluid would vary original direction and four vortexes are eventually formed within the drop.

Figure 7a illustrates that the temperature turns out to be more uniformly distributed arising from the Marangoni flow within drop as time increases, which consequently make the flow patterns varied. For 0.10 s of time, the temperature gradients on right and left surfaces have basically the same level, and different parts are also less different in velocity, as presented in Figure 7b. For 0.20 s and 0.30 s of time, the temperature gradients on right surface tend to surmount those on the left, and the velocity on left surface is smaller than that on the right. The stagnation points would slowly move to the left, and left vortex would be shrunk, in contrast to t =0.10 s. For 0.40 s of time, the temperature gradients merely takes on one end, which makes the fluid moved from one side to the other, and only one stagnation point exists, as illustrated in Figure 6. As a result, the two vortexes would eventually appear inside the water drop. The small interface velocity pulsation would be induced, and the

pulsation intensity turns to be very small, though the middle part of droplet surface takes on very smaller temperature gradients. Internal circulations within the droplet are seldom effected by the velocity pulsation, and appear stable state.

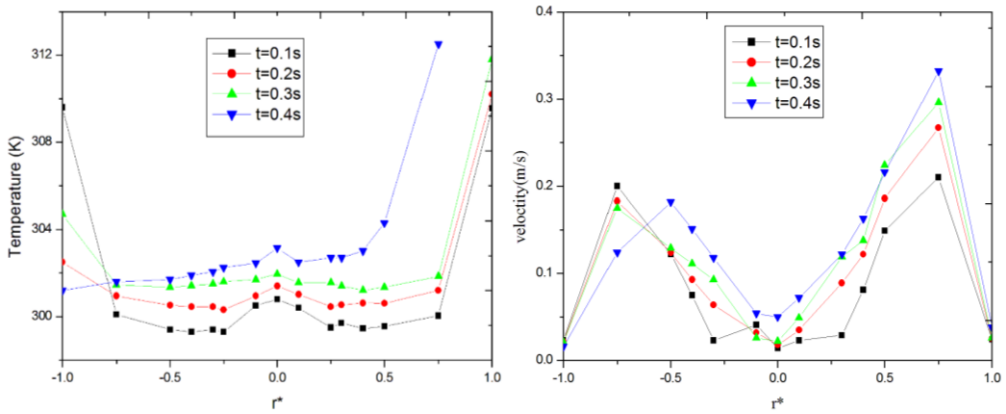

(a) Temperature distributions (b) velocity distributions

Figure 7: Temperature and velocity on drop surface (a) Temperature distributions and (b) velocity distributions

4 Conclusions

A combined Volume of Fluid (VOF) method and Continuum Surface Force (CSF) model are presented to calculate the unsteady internal flow within a drop suspending under high-temperature environment. The Marangoni effects are substantially conducive to the evaporation rate and are not neglected in droplet evaporating. Unsteady internal flow is induced by temperature gradients on droplet surface. Four vortexes are converted into double axisymmetric vortexes with evaporating of droplet, due to stagnation point from two to one arising from the viscous force inner droplet. Marangoni flow makes the temperature more uniformly distributed, and the heat transfer is facilitated. Furthermore, Marangoni flow gradually weakens due to uniform temperature distribution. These results lay the valuable foundation for probing into the unsteady flow in droplet evaporation with Marangoni effects.

Acknowledgments: The authors wish to acknowledge the research grant from National Natural Science Foundation of China (No.51106064) and Natural Science Foundation of Jiangsu Province, China (No. BK20171301, BK20150511), a project funded by the Priority Academic Program Development of Jiangsu Higher Education Institutions (PAPD) and a project supported by Jiangsu University for NSFC (FCJJ2015001).

References

Bénard, H. (1901): Les tourbillons cellulaires dans une nappe liquide transportant de la chaleur par convection en régime permanent. *Annales de Chimie Physique*, vol. 23, pp. 62-144.

Block, M. J. (1956): Surface tension as the cause of Bénard cells and surface deformation in a liquid film. *Nature*, vol. 178, no. 4534, pp. 650-651.

Brackbill, J. U.; Kothe, D. B.; Zemach, C. (1992): A continuum method for modeling surface-tension. *Journal of Computational Physics*, vol. 100, no. 2, pp. 335-354.

Buffone, C.; Sefiane, K. (2004): Investigation of thermocapillary convective patterns and their role in the enhancement of evaporation from pores. *International Journal of Multiphase Flow*, vol. 30, no. 9, pp. 1071-1091.

Chen, W. H. (2001): Unsteady absorption of sulfur dioxide by an atmospheric water droplet with internal circulation. *Atmospheric Environment*, vol. 35, no. 13, pp. 2375-2393.

Gao, P.; Yin, Z.; Hu, W. (2008): Thermocapillary motion of droplets at large Marangoni numbers. *Advances in Space Research*, vol. 41, no.12, pp.2101-2106.

Gleason, K.; Voota, H.; Putnam, S. A. (2016): Steady-state droplet evaporation: Contact angle influence on the evaporation efficiency. *International Journal of Heat and Mass Transfer*, vol.101, pp. 418-426.

Girard, F.; Antoni, M.; Faure, S.; Steinchen, A. (2006): Evaporation and Marangoni driven convection in small heated water droplets. *Langmuir*, vol. 22, no. 26, pp. 11085-11091.

Girard, F.; Antoni, M.; Sefiane, K. (2008): On the effect of Marangoni flow on evaporation rates of heated water drops. *Langmuir*, vol. 24, no. 17, pp. 9207-9210.

Grove, A. S.; Shair, F. H.; Petersen, E. E.; Acrivos, A. (1964): An experimental investigation of the steady separated flow past a circular cylinder. *Journal of Fluid Mechanics*, vol. 19, no. 1, pp. 60-85.

He, B.; Duan, F. (2015): Evaporation and convective flow pattern of a heated pendant silicone oil droplet. *International Journal of Heat and Mass Transfer*, vol. 85, pp. 910-915.

Hegseth, J. J.; Rashidnia, N.; Chai, A. (1996): Natural convection in droplet evaporation. *Physical Review E*, vol. 54, no. 2, pp. 1640-1644.

Hirt, C. W.; Nichols, B. D. (1981): Volume of Fluid (VOF) method for the dynamics of free boundaries. *Journal of Computational Physics*, vol. 39, no. 1, pp. 201-225.

Hu, H.; Larson, R. G. (2005): Analysis of the effects of Marangoni stresses on the micro flow in an evaporating sessile droplet. *Langmuir*, vol. 21, no. 9, pp. 3972-3980.

Lu, G.; Duan, Y. Y.; Wang, X. D.; Lee, D. J. (2011): Internal flow in evaporating droplet on heated solid surface. *International Journal of Heat and Mass Transfer*, vol. 54, no. 19-20, pp. 4437-4447.

Mandal, D. K.; Bakshi. S. (2012): Internal circulation in a single droplet evaporating in a closed chamber. *International Journal of Multiphase Flow*, vol. 42, pp. 42-51.

Niazmand, H.; Shaw, B. D.; Dwyer, H. A.; Aharon, I. (1994): Effects of Marangoni convection on transient droplet evaporation. *Combustion Science and Technology*, vol. 103, pp. 219-233.

Park, K.; Lee, K. S. (2003): Flow and heat transfer characteristics of the evaporating extended meniscus in a micro-capillary channel. *International Journal of Heat and Mass Transfer*, vol. 46, no. 24, pp. 4587-4594.

Pearson, J. R. A. (1958): On convection cells induced by surface tension. *Journal of Fluid Mechanics*, vol. 4, no. 5, 489-500.

Prakash, S.; Sirignano, W. A. (1978): Liquid fuel droplet heating with internal circulation. *International Journal of Heat and Mass Transfer*, vol. 21, no. 7, pp. 885-895.

Rybdylova, O.; Poulton, L.; Qubeissi, M. A.; Elwardany, A. E. et al. (2018): A model for multi-component droplet heating and evaporation and its implementation into ANSYS Fluent. *International Communications in Heat and Mass Transfer*, vol. 90, pp. 29-33.

Savino, R.; Fico, S. (2004): Transient Marangoni convection in hanging evaporating drops. *Physics of Fluids*, vol. 16, no. 10, pp. 3738-3754.

Savino, R.; Paterna, D.; Favaloro, N. (2002): Buoyancy and Marangoni effects in an evaporating drop. *Journal of Thermophysics and Heat Transfer*, vol. 16, no. 4, pp. 562-574.

Schlottke, J.; Weigand, B. (2008): Direct numerical simulation of evaporating droplets. *Journal of Computational Physics*, vol. 227, no. 10, pp. 5215-5237.

Shih, A. T.; Megaridis, C. M. (1996): Thermocapillary flow effects on convective droplet evaporation. *International Journal of Heat and Mass Transfer*, vol. 39, no. 2, pp. 247-257.

Soltani, N.; Rahal S. (2017): Control of the convective flow instabilities in a simulated Czochralski growth system. *Fluid Dynamics & Material Processing*, vol. 13, no. 1, pp. 1-17.

Wang, Z.; Guo, T.; Tian, L.; Xu, Q.; Zhan, S. et al. (2017): Numerical simulation on circulation flow and mass transfer inside atmospheric water drops. *Applied Thermal Engineering*, vol. 118, pp. 765-772.

Xu, X.; Luo, J. (2007): Marangoni flow in an evaporating water droplet. *Applied Physics Letters*, vol. 91, no. 12, pp. 124102.

Zhang, N.; Yang, W. J. (1992): Natural-convection in evaporating minute drops. *Journal of Heat Transfer-Transactions of the ASME*, vol. 104, no. 4, pp. 656-662.

Zhu, Z. Q.; Brutin, D.; Liu, Q. S.; Wang, W.; Mourembles, A. et al. (2010): Experimental investigation of pendant and sessile drops in microgravity. *Microgravity Science and Technology*, vol. 22, no. 3, pp. 339-345.